Calcif. Tiss. Res. 24, 19–27 (1977)

Calcified
Tissue Research

Stages in the Dissolution of Human Enamel Crystals in Dental Caries

J.C. Voegel and R.M. Frank

Centre de Recherches, Faculté de Chirurgie Dentaire, Université Louis Pasteur, 1, Place de l'Hôpital, F-67000, Strasbourg, France

Summary. Various stages in monocrystal dissolution occurring during human enamel caries were studied by high resolution transmission electron microscopy. After the development of a central core lesion, two mechanisms by which the dissolution spread laterally to the (100) faces of the crystal could be demonstrated on the basis of the systematic orientation of the crystallographic axes. In the first case, the destruction was developing parallel to (120) planes and the borders were limited by (100) planes. In the second type, the development of the lateral side lesion was observed parallel to (100) planes. The carious destruction of the enamel monocrystal occurred as a result of the development of several lateral side dissolutions of the two types described, proceeding along the entire central core lesion.

Key words: Dissolution — Crystallographic axes — (100) planes — Dislocation.

Introduction

High resolution transmission electron microscopy has demonstrated the presence of periodicities within sectioned biological apatite crystals. These periodic structures can be considered as a direct resolution of the crystal lattice (Selvig, 1970, 1972, 1973). After acid attack of synthetic apatite crystals, a preferential dissolution of the central crystalline core was shown with this observation method and with the scanning electron microscope (Arends et al., 1973; Jongebloed et al., 1974). Similarly, the formation of central holes in human enamel crystals during the carious process was observed by Swancar et al. (1969), Voegel and Frank (1974), and Jongebloed et al. (1975).

Welch (1968) and Arends et al. (1971) assumed that the presence of dislocations parallel to the *c* axis was the main reason for central core lesions during apatite crystal dissolution.

In the present study, various steps in carious monocrystal dissolution were studied in human enamel, in relation to the crystallographic axes.

Material and Methods

Carious human enamel was obtained from premolars and permanent molars in 14–30-year-old patients. Enamel from white spots without cavitation, as well as from advanced enamel lesions, fragmented in small blocks, were fixed for 3 h in a 2% glutaraldehyde-paraformaldehyde solution in a 0.1 M cacodylate buffer at pH 7.4. After a 1 h post-fixation in a 2% osmic acid solution in the same buffer, the fragments were embedded in Epon 812. Non-decalcified thin sections of about 200–300 Å in thickness were obtained with a Servall-Porter microtome equipped with a diamond knife and examined in a Jeol 100 B transmission electron microscope using a special cathode, a low-beam current, and an anticontamination system under a tension of 100 kV. The equidistances of the different planes were obtained by the mean value of about 20 parallel fringes. For the analysis of the lattice patterns and the determination of the dimension of the central holes, the instrument magnification was corrected when necessary using the 8.17 Å spacing of the d_{100} lattice fringe.

Results

In typical enamel caries, the crystal dissolution was more advanced in the prism region than in the interprismatic substance (Fig. 4). A diffuse attack of the crystals was observed and intact monocrystals could be observed among dissolving crystals (Figs. 5 and 12).

The direct demonstration of periodic striations with high resolution transmission electron microscopy allowed us to follow the different stages of the carious

Send offprint requests to R. Frank at the above address

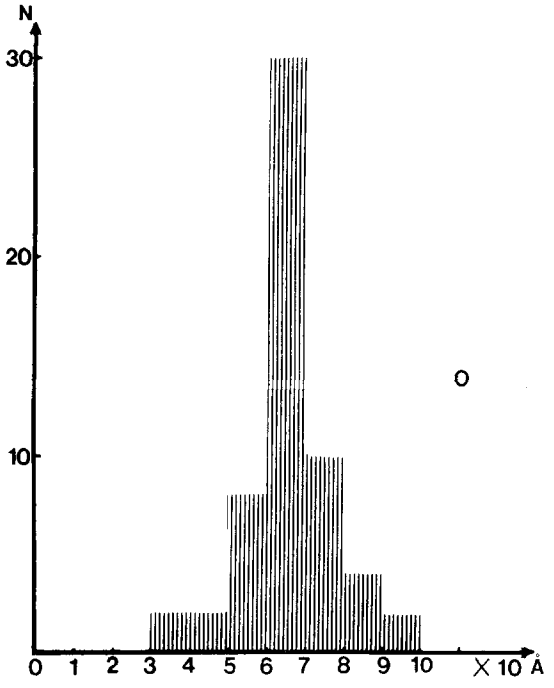

Fig. 1. Size distribution of the central core lesions measured perpendicularly to (100) planes before the appearance of lateral destructions

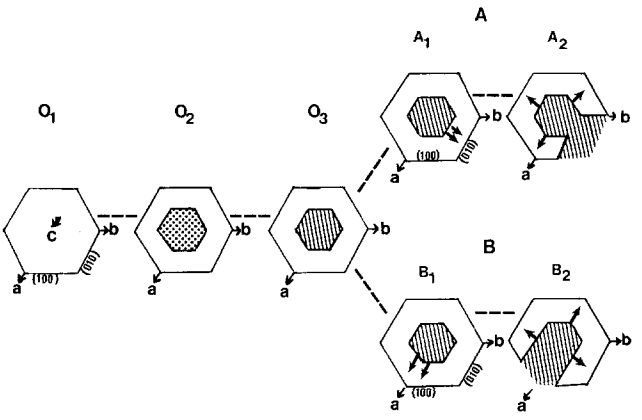

Fig. 2. Diagrammatic representation of the different steps of the monocrystal dissolution seen in directions perpendicular to the *c* axis

dissolution at the monocrystalline level. The apatite crystal destruction always began at the extremities of the monocrystal (Figs. 2 and 3: step O_1) leading to the formation of a central hole, often hexagonal in cross-section. These lesions were limited by the (100) planes (Figs. 2 and 3: step O_2). In short order the dissolution extended along the central core of the crystal along the *c* axis (Figs. 2 and 3: step O_3; and Figs. 6, 9, 10, and 12). Systematic measurements of the width of the central holes perpendicular to the (100) planes have been made at this stage (Fig. 1). Values between 30 and 100 Å were recorded with maximum frequency between 60 and 70 Å. This maximum corresponded approximately to $8d_{100}$ (d_{100} = equidistance of (100) planes).

After the formation of the central hole, the dissolution extended towards the (100) and equivalent faces of

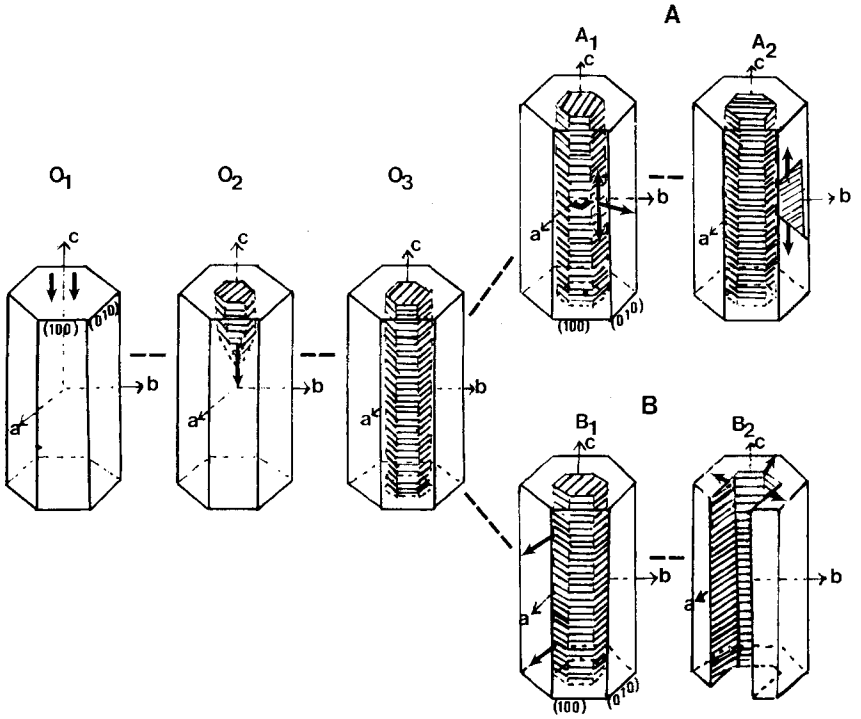

Fig. 3. Diagrammatic representation of the different steps of monocrystal dissolution seen in a direction parallel to the *c* axis

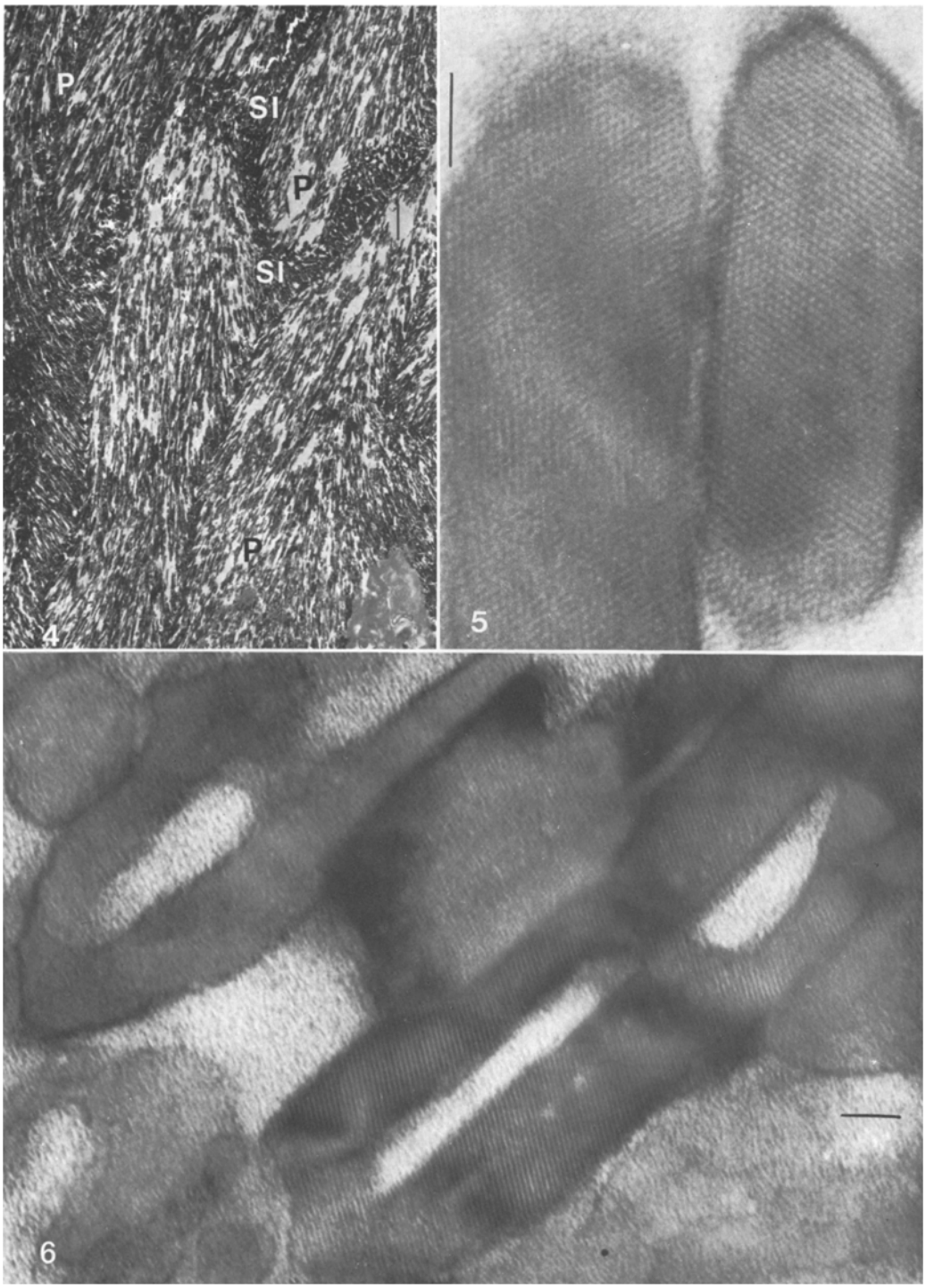

Fig. 4. Overall view of a carious enamel region. The dissolution of the monocrystals is more advanced in the prism (*P*) than in the interprismatic substance (*SI*). ×6000
Fig. 5. Three series of fringes corresponding to (100) planes are visible in two intact enamel monocrystals. ×1,400,000
Fig. 6. A central core dissolution of enamel monocrystals is observed during the carious process. ×850,000

the monocrystal according to two different crystallographic procedures. The beginning of the lateral side destruction has often been observed (Figs. 11 and 16). In the first type of lateral dissolution (mechanism A), the destructive process followed a direction parallel to (120) planes (Figs. 2 and 3: step A_1). The edges of

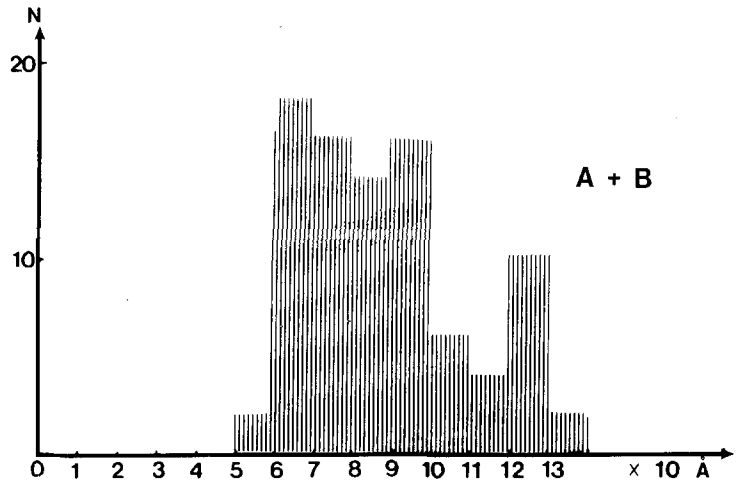

Fig. 7. Size distribution of the central core lesions after development of one of the lateral crystal dissolutions

the destruction were limited by (100) and (010) planes (Figs. 2 and 3: step A_2; Figs. 12–15). A progression of the dissolution parallel to the *c* axis has been clearly shown. However, it is difficult to define it by typical crystallographic planes.

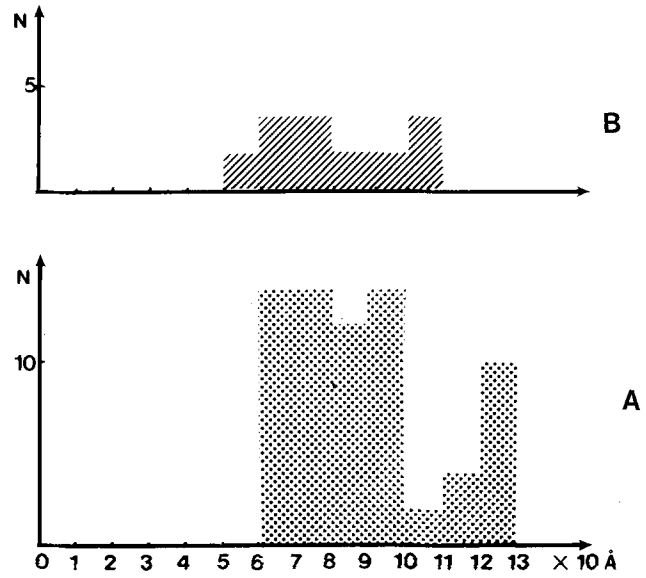

Fig. 8. A: Size distribution of the central core lesions after the appearance of lateral diffusion perpendicular to (100) planes. B: Size distribution of the central core lesions after the appearance of lateral diffusion parallel to (100) planes

In the second type of lateral dissolution (mechanism B), localized destructions towards the (100) or equivalent faces of the crystal developed parallel to the *a* or *b* axis (Figs. 2 and 3: steps B_1 and B_2; and Figs. 16–18). By measuring systematically the central hole sizes in a direction perpendicular to (100) planes after development of any one of the lateral side dissolutions, values comprising between 50 Å and 130 Å with a maximum distribution between 60 and 100 Å (Fig. 7) were obtained. These latter values were approximately equivalent to $8–11 d_{100}$.

When studying separately the size distribution of the lateral crystalline dissolution by either mechanism A or B (Fig. 8), the relative frequency of each dissolution type can be deduced. It appeared that the lateral A type destruction perpendicular to the (100) planes was observed four times more frequently than the B type. In mechanism A, the values ranged from 60 Å to 130 Å. For mechanism B, the values varied less from 50 Å to 110 Å.

By progressive development of the lateral dissolution process, the central loss of inorganic material was extended, creating lateral openings either unilaterally (Figs. 13–16, and 18) or on several sides (Fig. 17). The development of several lateral extensions through mechanism A or B led to the fragmentation of the monocrystal and to the disappearance of important parts of the crystalline shell (Figs. 19 and 20).

Thus, the total destruction of the enamel monocrystal during the carious process is the result of the lateral extension of the dissolution perpendicular and parallel to (100) planes.

Discussion

At the ultrastructural level, the carious process in prismatic enamel started at the interface between the prism and the interprismatic substance by an apatite crystal dissolution leading to a widening of the "prismatic sheath" (Frank, 1973; Frank and Voegel, 1975). A scattered crystalline and diffuse destruction was then observed in the prismatic region, the interprismatic substance (Fig. 4) being spared until the last stage.

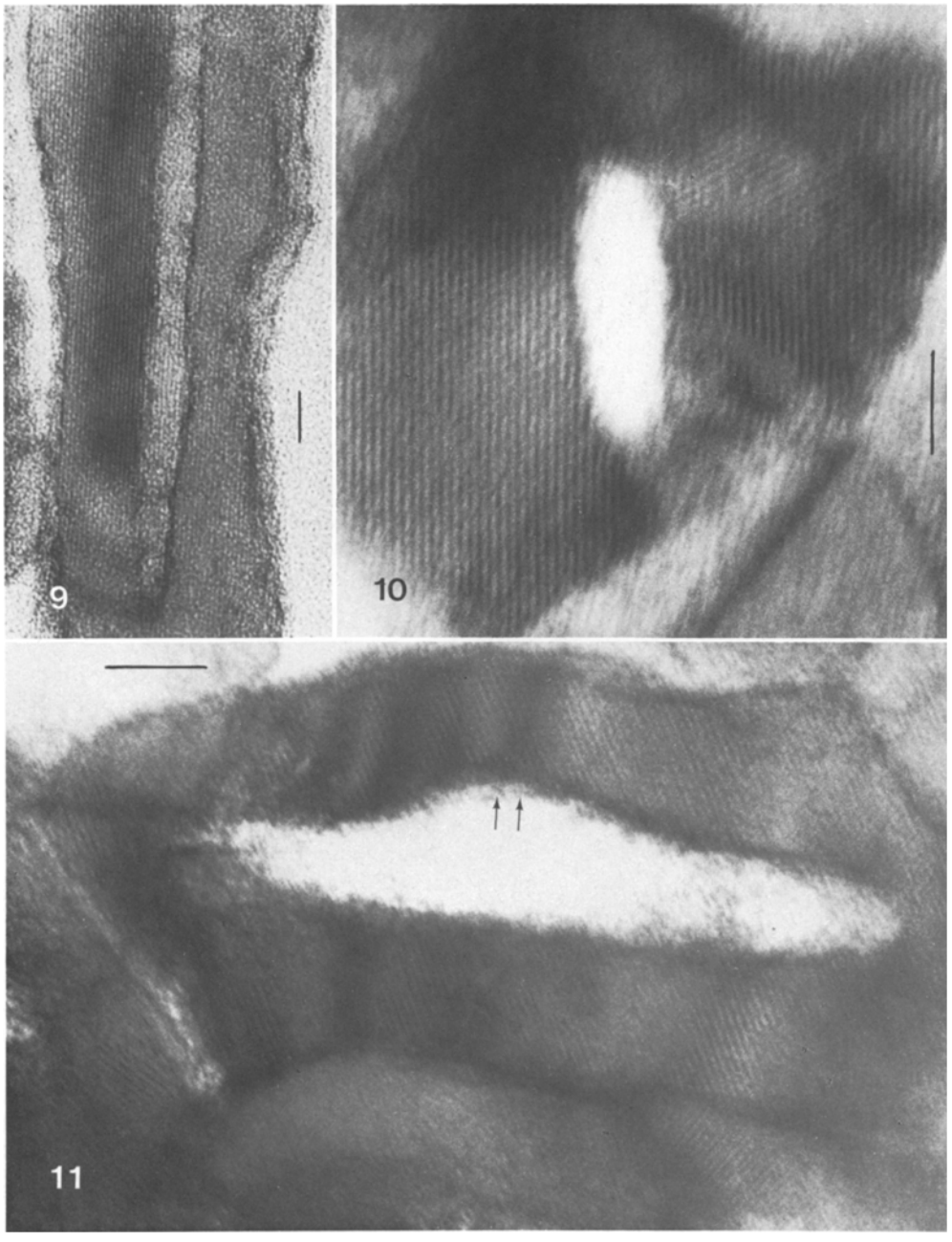

Fig. 9. Central core lesion appearing parallel to (100) planes in the first step of the monocrystal dissolution. ×700,000

Fig. 10. First stage of the central core dissolution with a small development along the *a* and *b* axes. Presence of (100) and (010) planes. ×1,450.000

Fig. 11. In a monocrystal, with a central core lesion, the beginning of the lateral dissolution (arrows) can be observed perpendicular to (100) planes. ×1,450,000

When studying the morphology of individual enamel monocrystals with high resolution transmission electron microscopy, the observed equidistant and parallel fringes can be considered as representing on the screen the arrangement of the atomic or molecular planes of the crystal (Fig. 5). In this study of the different steps of carious enamel crystal dissolution, only such pictures showing simultaneously two sets of planes in the same crystal were used. Thus the shape of the monocrystal, the plane of section, and the development of the carious dissolution could be unequivocally related to the crystallographic axes.

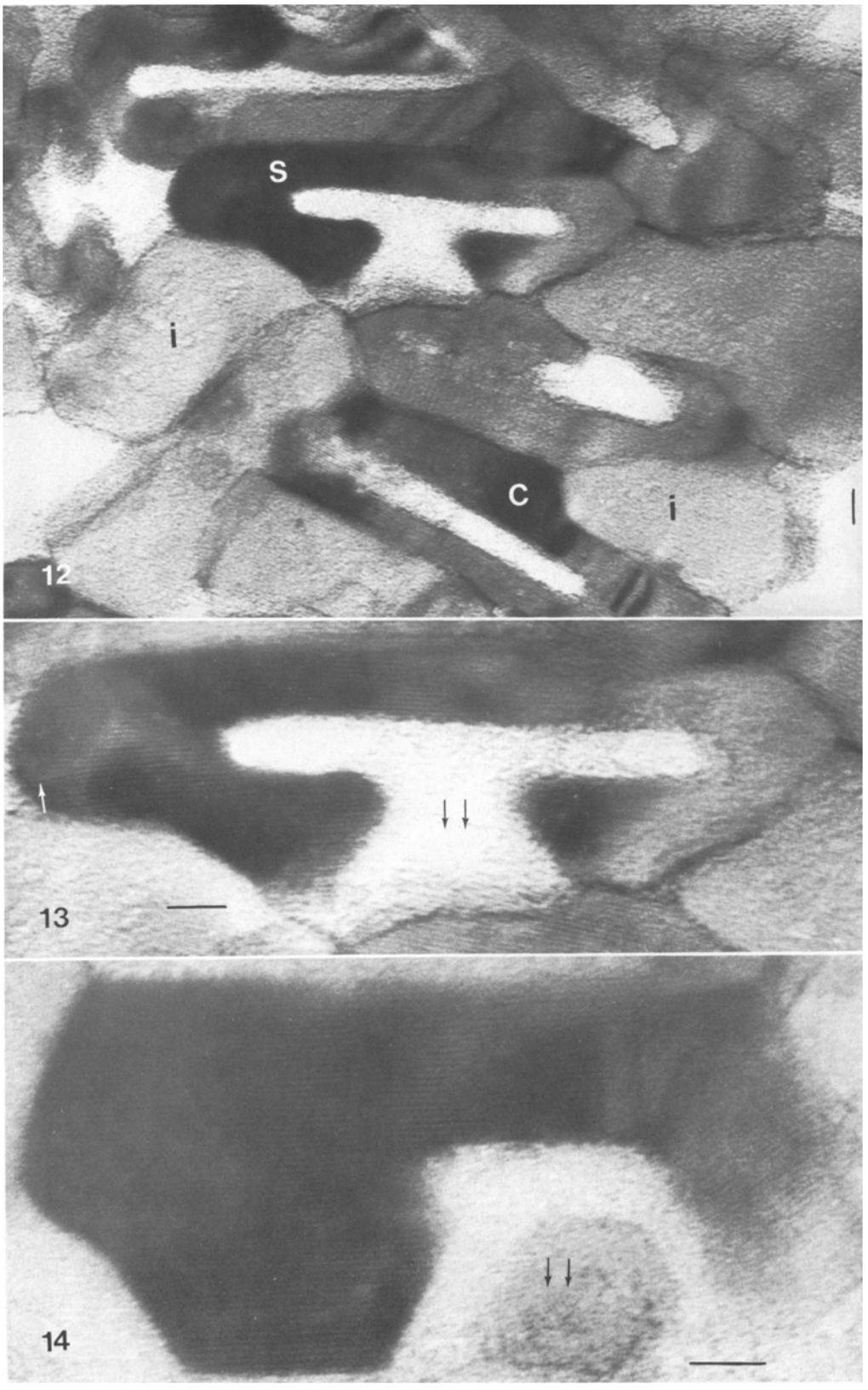

Fig. 12. Overall view of an enamel carious area. Apparently intact crystals (*I*) can be seen among crystals with central core lesions (*C*). Some crystals show, in addition, lateral side destruction (*S*). ×520,000

Fig. 13. Monocrystal with carious dissolution development perpendicular to (100) planes. The characteristic lateral side aperture is present (*black arrows*). A supplementary half plane produced by dislocation is visible (*white arrow*). ×920,000

Fig. 14. Carious enamel monocrystal showing the lateral side A type of dissolution. ×1,150,000

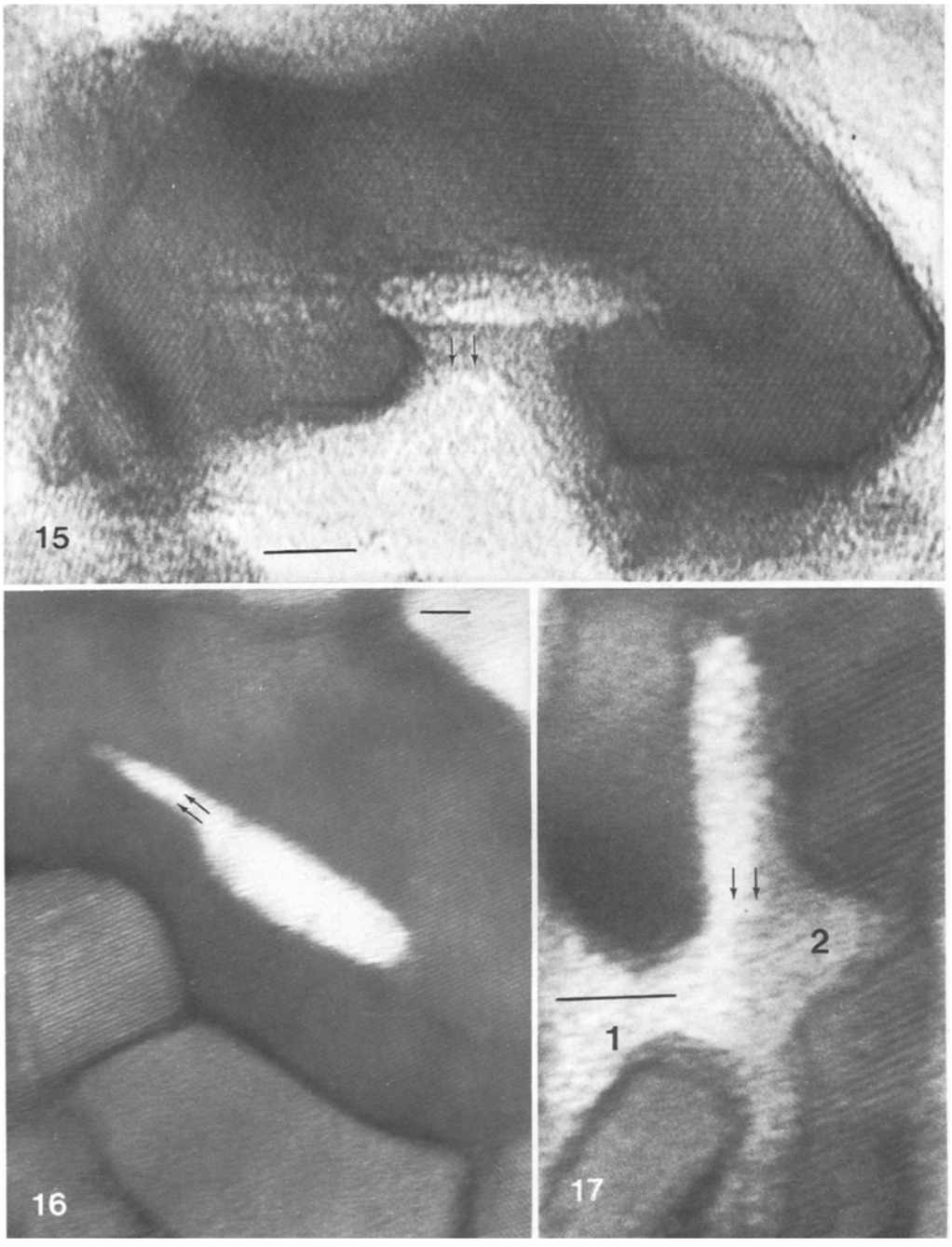

Fig. 15. Carious enamel monocrystal dissolution. The *black arrows* indicate the dissolution perpendicular to (100) planes (A type). The borders of the lateral side aperture are limited by (100) planes. ×1,350,000

Fig. 16. First stage (*black arrows*) of development parallel to (100) planes leading to the formation of a lateral side aperture of Type B. Note the close contact between the crystals. ×720,000

Fig. 17. Enamel carious monocrystal with a central core lesion (*arrows*) as well as a complete lateral side destruction (*1*) and the beginning (*2*) of another lateral lesion perpendicular to (100) planes on the opposite side. ×1,700,000

In all cases, the dissolution started at one extremity of the monocrystal to form a hole, often hexagonal, extending anisotropically along the *c* axis, in agreement with the observations of Swancar et al. (1969), Arends et al. (1975), and Voegel and Frank (1974). This central core lesion could be influenced by helicoidal defects oriented parallel to the *c* axis (Arends et al., 1971; Jongebloed et al., 1974). These defects might be present in the whole apatite family. This hypothesis seemed to be confirmed by our own observations,

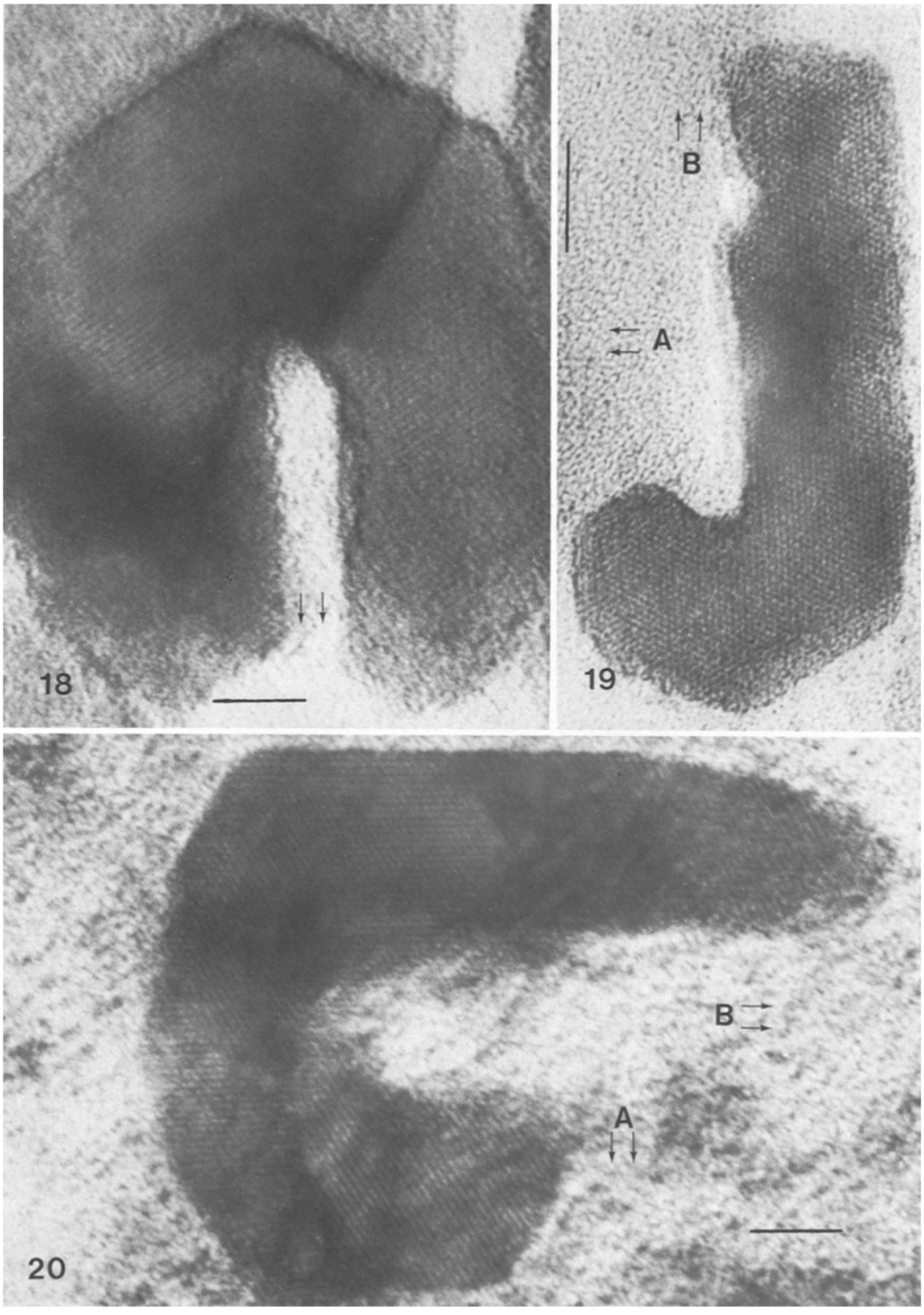

Fig. 18. Side aperture formation (*black arrows*) obtained by diffusion along (100) planes. ×1,360,000

Fig. 19. Advanced destruction of the monocrystal by combination of the two types of dissolution perpendicular (*A*) or parallel (*B*) to (100) planes. ×1,120,000

Fig. 20. Carious enamel monocrystal dissolved by the combination of *A* and *B* mechanisms. ×1,300,000

especially by (1) the rapid and anisotropic extension of the crystalline destruction along and parallel to the *c* axis, (2) the development of the dissolution parallel to the outer hexagonal faces, and (3) the presence of a crystalline defect consisting at the fringe level of a supplementary half plane (Fig. 13) produced either by a

Taylor-Orowan dislocation (edge dislocation) or a screw dislocation. It must also be considered that screw dislocations are the basis of the helicoidal growing theory of the monocrystals.

The study of the dissolution width measured perpendicular to (100) planes during the initial steps of dissolution showed no central holes smaller than 30 Å (corresponding approximately to $4d_{100}$) in diameter. The dissolution front therefore progressed with this width. The maximum values of the central hole sizes ranged from 60 Å and 70 Å in width. Along the *a* or *b* axis, the dissolution was stopped after the involvement of nearly 8 (100) planes. Jongebloed et al. (1975) showed that a crystal having an original size of 400 Å will produce, after acid treatment in vitro, two crystals of about 150 Å. These results suggested that the in vitro produced central holes had a diameter of about 100 Å, a value which is in agreement with our own findings obtained on enamel crystals subject to the carious process.

The second and ultimate step of dissolution could be accurately described, taking into account the systematic orientation of the crystallographic planes within the monocrystals. The lateral side extension developing perpendicular to the *a* or *b* axis (Figs. 2 and 3: mechanism A) penetrated only slightly along the *c* axis and led to the formation of a cone-shaped lateral destruction (Figs. 2 and 3: steps A_1 and A_2). It seemed more than likely that the extension of the dissolution progressed parallel to the *c* axis (Figs. 2 and 3: step A_2). The sizes of the central holes measured after the occurrence of the lateral A type of side destruction showed clearly a distribution between 60 and 110 Å. Such a distribution corresponded either to a slow dissolution rate of the lateral side destructions or to the appearance of these later after a complete and total development of the central hole lesion. The other type (Figs. 2 and 3: mechanism B) of lateral destruction parallel to the *a* or *b* axis occurred through a localized extension of the central hole formation by a side destruction parallel to (100) planes. A large side aperture spreading through the whole crystal appeared (Figs. 2 and 3: steps B_1 and B_2). Final stages of attack perpendicular to (100) planes seemed to be highly probable as well as combinations of A and B types of side dissolution (Figs. 19 and 20).

After acid treatment of single crystals of synthetic hydroxyapatite, Jongebloed (1974) showed a type of defect which could possibly be related to lateral dissolution. In carious enamel, chemical analysis has shown an enrichment in HPO_4^{2-} ions when compared to normal enamel (Arends and Davidson, 1975). A preferential loss of carbonate ions has also been observed in incipient carious lesions (Hallsworth et al., 1973). It will be interesting in the future to correlate these chemical findings with the different steps of the carious monocrystal destruction. This will aid in the identification of the preferential sites of dissolution within the enamel monocrystal during the carious process.

References

Arends, J., Royce, B.S.H., Welch, D.O., Smoluchowski, R.: Lattice defects and the electrical and transport properties of apatite. In: Int. symp. on the structural properties of hydroxyapatite (Young, R.A., ed.). New York: Benjamin 1971

Arends, J., Davidson, C.L.: HPO_4^{2-} content in enamel and artificial carious lesions. Calcif. Tiss. Res. **18**, 65–79 (1975)

Arends, J., Berg, P.J. van den, Jongebloed, W.L.: Dissolution of hydroxyapatite single crystals. In: Physico-chimie et cristallographie des apatites d'intérêt biologique. Colloque CNRS No. 230, pp. 389–395. Paris: 1973

Frank, R.M.: Microscopie électronique de la carie des sillons chez l'Homme. Archs. Oral Biol. **18**, 9–25 (1973)

Frank, R.M., Voegel, J.C.: Etude ultrastructurale de la dissolution des cristaux d'apatite au cours de la carie de l'émail dentaire humain. In: Physicochimie et cristallographie des apatites d'intérêt biologique. Colloque CNRS No. 230, pp. 369–380. Paris: 1975

Hallsworth, A.S., Weatherell, J.A., Robinson, C.: Loss of carbonate during the first stage of enamel caries. Caries Res. **7**, 345–348 (1973)

Jongebloed, W.L., Berg, P.J. van den, Arends, J.: The dissolution of single crystals of hydroxyapatite in citric and lactic acids. Calcif. Tiss. Res. **15**, 1–9 (1974)

Jongebloed, W.L., Molenaar, I., Arends, J.: Morphology and size distribution of sound and acid treated enamel crystallites. Calcif. Tiss. Res. **19**, 109–123 (1975)

Selvig, K.A.: Periodic lattice images of hydroxyapatite crystals in human bone and dental hard tissues. Calcif. Tiss. Res. **6**, 227–238 (1970)

Selvig, K.A.: The crystal structure of hydroxyapatite in dental enamel as seen with the electron microscope. J. Ultrastruct. Res. **41**, 369–375 (1972)

Selvig, K.A.: Electron microscopy of dental enamel: Analysis of crystal lattice images. Z. Zellforsch. **137**, 271–281 (1973)

Swancar, J.R., Scott, D. B., Simmelink, J.W., Smith, T.J.: The morphology of enamel crystals. In: Tooth enamel (Fearnhead R.W. and Stack M.V., eds.), vol. 2, pp. 233–239. Bristol: Wright 1969

Voegel, J.C., Frank, R.M.: Microscopie électronique de haute résolution du cristal d'apatite d'émail humain et de sa dissolution carieuse. J. Biol. Buccale **2**, 39–50 (1974)

Welch, D.: Defect structures in apatite. In: Physical and biological properties of apatite, pp. 13–24. Princetown University Conference, May 1968

Received March 26, 1976 / Accepted January 10, 1977